

Thickness-dependent electronic and magnetic properties of γ' -Fe₄N atomic layers on Cu(001)

Y. Takahashi,¹ T. Miyamachi,^{1,*} S. Nakashima,¹ N. Kawamura,^{1,2} Y. Takagi,^{3,4}
M. Uozumi,^{3,4} V. Antonov,^{5,6} T. Yokoyama,^{3,4} A. Ernst,⁵ and F. Komori^{1,†}

¹*Institute for Solid State Physics, The University of Tokyo, Kashiwa, Chiba 277-8581, Japan*

²*Science & Technology Research Laboratories, NHK, Setagaya, Tokyo 157-8510, Japan*

³*Department of Materials Molecular Science, Institute for Molecular Science, Myodaiji-cho, Okazaki 444-8585, Japan*

⁴*Department of Structural Molecular Science, The Graduate University for
Advanced Studies (SOKENDAI), Myodaiji-cho, Okazaki 444-8585, Japan*

⁵*Max-Planck-Institut für Mikrostrukturphysik, Weinberg 2, 06120 Halle, Germany*

⁶*Institute for Metal Physics, 36 Vernadsky Street, 03142 Kiev, Ukraine*

Growth, electronic and magnetic properties of γ' -Fe₄N atomic layers on Cu(001) are studied by scanning tunneling microscopy/spectroscopy and x-ray absorption spectroscopy/magnetic circular dichroism. A continuous film of ordered trilayer γ' -Fe₄N is obtained by Fe deposition under N₂ atmosphere onto monolayer Fe₂N/Cu(001), while the repetition of a bombardment with 0.5 keV N⁺ ions during growth cycles results in imperfect bilayer γ' -Fe₄N. The increase in the sample thickness causes the change of the surface electronic structure, as well as the enhancement in the spin magnetic moment of Fe atoms reaching $\sim 1.4 \mu_B$ /atom in the trilayer sample. The observed thickness-dependent properties of the system are well interpreted by layer-resolved density of states calculated using first principles, which demonstrates the strongly layer-dependent electronic states within each surface, subsurface, and interfacial plane of the γ' -Fe₄N atomic layers on Cu(001).

PACS numbers: 68.37.Ef, 71.15.Mb, 78.70.Dm, 78.20.Ls

I. INTRODUCTION

Iron nitrides, especially in iron-rich phases, have been under intense research due to the strong ferromagnetism and interest in its physical origin^{1,2}. The difficulty in obtaining a single phase has been a long-standing problem for ferromagnetic iron nitrides, to hinder fundamental understanding of intrinsic physical properties³⁻⁵. Recently, the successful epitaxial growth of single-phase ferromagnetic γ' -Fe₄N has been reported on various substrates, which helps to comprehend a crucial role for the hybridization between Fe and N states in the ferromagnetism of γ' -Fe₄N⁶⁻¹². The robust Fe-N bonding also renders an Fe₂N layer strongly two-dimensional¹³, which possibly facilitates a layer-by-layer stacking of γ' -Fe₄N on metals. This contrasts with the case of elemental 3d transition metals (TMs) deposited on 3d TM substrates, in which inevitable atom intermixing and exchange of constituents prevent the formation of ordered overlayers¹⁴⁻¹⁶. Therefore, the investigation into the electronic and magnetic states of γ' -Fe₄N atomic layers can not only elucidate the layer-/site-selective electronic and magnetic states of γ' -Fe₄N, but unravel the origin of the strongly thickness-dependent physical properties in a thin-film limit of 3d TM ferromagnets¹⁷⁻²⁴.

Here, we report two growth modes of γ' -Fe₄N/Cu(001) depending on preparation methods. The scanning tunneling microscopy/spectroscopy (STM/STS) observations indicated a successful growth of ordered trilayer γ' -Fe₄N, without extra nitrogen bombardment onto the existing structures. X-ray absorption spectroscopy/magnetic circular dichroism (XAS/XMCD) measurements revealed the thickness dependence of the

magnetic moments of Fe atoms, the origin of which was well explained by the first-principles calculations. Based on an atomically-resolved structural characterization of the system, the layer-by-layer electronic and magnetic states of the γ' -Fe₄N atomic layers have been understood from both experimental and theoretical points of view.

II. METHODS

A clean Cu(001) surface was prepared by repetition of sputtering with Ar⁺ ions and subsequent annealing at 820 K. Iron was deposited at room temperature (RT) in a preparation chamber under an ultrahigh vacuum (UHV) condition ($< 1.0 \times 10^{-10}$ Torr), using an electron-bombardment-type evaporator (EFM, FOCUS) from a high-purity Fe rod (99.998 %). The STM measurements were performed at 77 K in UHV ($< 3.0 \times 10^{-11}$ Torr) using electrochemically etched W tips. The differential conductance dI/dV was recorded for STS using a lock-in technique with a bias-voltage modulation of 20 mV and 719 Hz. The XAS and XMCD measurements were performed at BL 4B of UVSOR-III^{25,26} in a total electron yield (TEY) mode. The degree of circular polarization was ~ 65 %, and the x-ray propagation vector lay within the (1 $\bar{1}$ 0) plane of a Cu(001) substrate. All the XAS/XMCD spectra were recorded at ~ 8 K, with external magnetic field B up to ± 5 T applied parallel to the incident x-ray. The symmetry and quality of the surface were also checked by low energy electron diffraction (LEED) in each preparation chamber. First-principles calculations

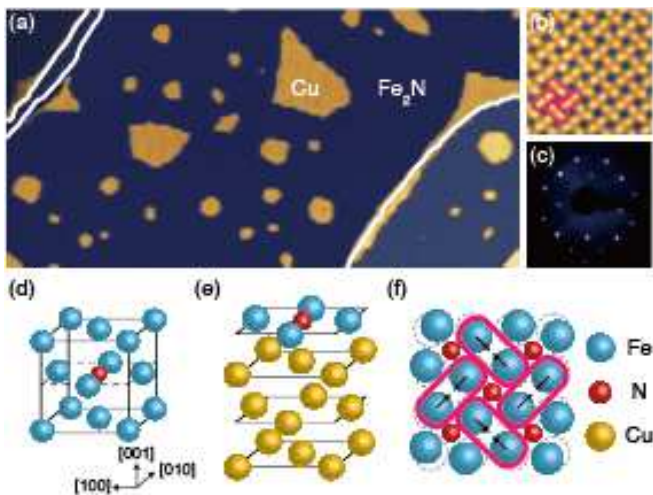


FIG. 1. (Color online) Topography and atomic structure of the monolayer γ' -Fe₄N on Cu(001). (a) Topographic image ($100 \times 50 \text{ nm}^2$, sample bias $V_s = +1.0 \text{ V}$, tunneling current $I = 0.1 \text{ nA}$) of the monolayer γ' -Fe₄N on Cu(001). White lines represent step edges of the Cu(001) terraces. Color contrast is enhanced within each terrace. (b) Close view ($2.5 \times 2.5 \text{ nm}^2$, $V_s = 0.25 \text{ V}$, $I = 45 \text{ nA}$) of the surface Fe₂N layer. The dimerization of Fe atoms is indicated by encirclement. (c) LEED pattern obtained with an incident electron energy of 100 eV . (d) Bulk crystal structure of γ' -Fe₄N. A dotted parallelogram represents an Fe₂N plane. (e) Atomic structure of the monolayer γ' -Fe₄N on Cu(001). (f) Schema illustrating $p4g(2 \times 2)$ reconstruction in the surface Fe₂N layer of γ' -Fe₄N. Arrows indicate the shift of the Fe atoms from an unreconstructed $c(2 \times 2)$ coordination (dotted circles). For (d) to (f), large blue (yellow) and small red spheres represent Fe (Cu) and N atoms, respectively.

were performed within the density functional theory in the local density approximation²⁷, using a self-consistent full-potential Green function method specially designed for surfaces and interfaces^{28,29}.

III. RESULTS AND DISCUSSION

A. Monolayer and bilayer-dot γ' -Fe₄N

Monolayer Fe₂N on Cu(001) was prepared prior to any growth of multilayer γ' -Fe₄N by the following cycle: N⁺ ion bombardment with an energy of 0.5 keV to a clean Cu(001) surface, subsequent Fe deposition at RT, and annealing at 600 K . Note that the monolayer Fe₂N is identical to Fe₄N on Cu(001) in a monolayer limit, and thus referred to as also "monolayer γ' -Fe₄N" hereafter. A topographic image of the sample after one growth cycle is shown in Fig. 1(a). The monolayer γ' -Fe₄N is formed on the Cu terraces at $\sim 0.85 \text{ ML}$ coverage. An atomically-resolved image of that surface displayed in Fig. 1(b) reveals a clear dimerization of the Fe atoms,

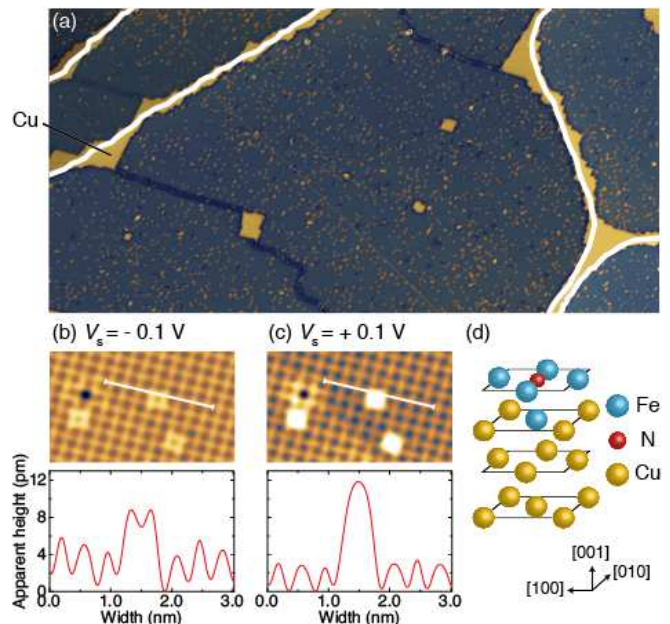


FIG. 2. (Color online) Topography of the bilayer γ' -Fe₄N dot on Cu(001). (a) Topographic image ($120 \times 60 \text{ nm}^2$, $V_s = -0.1 \text{ V}$, $I = 0.1 \text{ nA}$) of the monolayer (darker area) and dot-like bilayer γ' -Fe₄N on Cu(001). White lines represent step edges of the Cu(001) terraces. Color contrast is enhanced within each terrace. (b,c) Upper panels: Atomically-resolved topographic images ($7 \times 3 \text{ nm}^2$, $I = 2.0 \text{ nA}$) taken at (b) $V_s = -0.1 \text{ V}$ and (c) $+0.1 \text{ V}$. Lower panels: Height profiles measured along lines indicated in the upper panels. (d) Proposed atomic structure of the bilayer-dot γ' -Fe₄N on Cu(001). Large blue (yellow) and small red spheres correspond to Fe (Cu) and N atoms, respectively.

typical of ordered γ' -Fe₄N on Cu(001)^{30,31}. A LEED pattern of the surface is shown in Fig. 1(c), which exhibits sharp spots with the corresponding $p4g(2 \times 2)$ symmetry. It is known that^{30–33} the topmost layer of the γ' -Fe₄N on Cu(001) always consists of the Fe₂N plane in a bulk Fe₄N crystal shown in Fig. 1(d). A schematic model of the monolayer γ' -Fe₄N is given in Fig. 1(e), composed of a single Fe₂N plane on Cu(001). Accordingly, the surface Fe₂N plane takes reconstruction to the $p4g(2 \times 2)$ coordination³⁰, in which the Fe atoms dimerize in two perpendicular directions as illustrated in Fig. 1(f).

After repeating the growth cycles, we found a new structure different from the monolayer γ' -Fe₄N. Figure 2(a) displays the surface after two growth cycles in total, namely, another cycle of the N⁺ ion bombardment, Fe deposition, and annealing onto the existing monolayer γ' -Fe₄N surface. Then, the surface becomes mostly covered with the monolayer γ' -Fe₄N, which contains a small number of bright dots. For a structural identification of these dots, we measured atomically-resolved topographic images and line profiles at different V_s as shown in Fig. 2(b) and 2(c). The dot structure imaged at $V_s = -0.1 \text{ V}$ reveals the dimerization of the Fe atoms

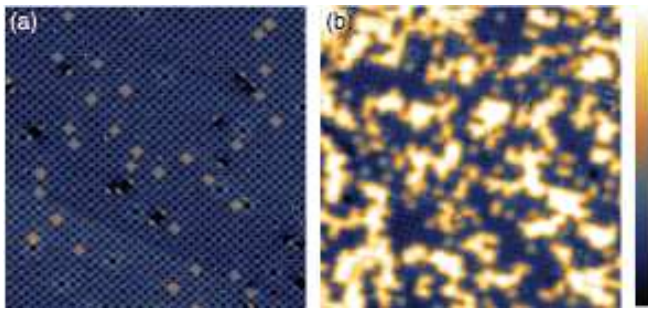


FIG. 3. (Color online) Topographic images ($15 \times 15 \text{ nm}^2$) of the surface after repetition of (a) two and (b) three growth cycles. The set point is $(V_s, I) = (+0.25 \text{ V}, 5.0 \text{ nA})$ for (a) and $(+0.1 \text{ V}, 3.0 \text{ nA})$ for (b).

as the monolayer γ' - Fe_4N surface. This indicates that the topmost part of the dot consists of the reconstructed Fe_2N . At positive V_s of $+0.1 \text{ V}$, in contrast, the dot is recognized as a single protrusion both in the topographic image and line profile, while the surrounding monolayer γ' - Fe_4N still shows the Fe dimerization. This implies the different electronic structure of the dot compared to the monolayer γ' - Fe_4N , which comes from the difference in a subsurface atomic structure.

The observed height difference between the dot and the monolayer γ' - Fe_4N ranges from 4 to 10 pm depending on V_s . These values are in the same order of a lattice mismatch between the bulk crystals of the γ' - $\text{Fe}_4\text{N}/\text{Cu}(001)$ (380 pm) and $\text{Cu}(001)$ (362 pm)³⁰, but an order of magnitude smaller than the lattice constant of the γ' - $\text{Fe}_4\text{N}/\text{Cu}(001)$. This suggests that the topmost layer of the dot is not located above the monolayer γ' - Fe_4N surface, but shares the Fe_2N plane with. Furthermore, the bright dot is composed of only four pairs of the Fe dimer as imaged in Fig. 2(b), indicating that the difference in the atomic and/or electronic structures is restricted within a small area. Considering the above, it is most plausible that one Fe atom is embedded just under the surface N atom at the dot center, and thus a bilayer γ' - Fe_4N dot is formed as schematically shown in Fig. 2(d). This structure corresponds to a minimum unit of the bilayer γ' - Fe_4N on $\text{Cu}(001)$.

This bilayer dot formed clusters by a further repetition of the growth cycles. Figure 3(a) shows an enlarged view of the iron-nitride surface after two growth cycles. The coverage of the dot is estimated to be $\sim 5 \%$ of the entire surface. Another growth cycle onto this surface led to an increase in a dot density up to $\sim 40 \%$, as shown in Fig. 3(b). However, further repetitions of the cycles resulted in neither a considerable increase in the dot density nor the formation of a continuous bilayer film. This can be attributed to an inevitable sputtering effect in every growth cycle: an additional N^+ ion bombardment to the existing surface not only implanted N^+ ions but also sputtered the surface, which caused the loss of the iron nitrides already formed at the

surface, as well as the increase in the surface roughness.

To compensate this loss of surface Fe atoms by the sputtering effect, we also tried to increase the amount of deposited Fe per cycle. Nonetheless, the number of Fe atoms, which remained at the surface after annealing, did not increase possibly because of the thermal metastability of Fe/Cu systems^{34–37}. The isolated Fe atoms without any bonding to N atoms were easily diffused and embedded into the Cu substrate during the annealing process. As a result, only the imperfect bilayer γ' - Fe_4N was obtained through this method.

B. Trilayer γ' - Fe_4N film

Multilayer γ' - Fe_4N films were obtained by the following procedure. First, the monolayer γ' - Fe_4N was prepared on $\text{Cu}(001)$ as above. Then, 2 ML Fe was deposited under N_2 atmosphere ($5.0 \times 10^{-8} \text{ Torr}$)³⁸ at RT, and the sample was annealed at 600 K. Figures 4(a) and 4(b) show topographic images after two and three above mentioned cycles, respectively. In the images, the coverage of new bright area, different from the imperfect bilayer dot, monotonously increases with repeating the cycles. A close view of that new surface is displayed in Fig. 4(c), revealing the dimerized (or even $c(2 \times 2)$ -like dot) structures. Because a LEED pattern shown in the inset of Fig. 4(c) exhibits the $p4g(2 \times 2)$ symmetry without extra spots, the topmost layer of this surface is composed of the reconstructed Fe_2N plane³¹. Therefore, these observations suggest that the new area would consist of γ' - Fe_4N other than both of the monolayer and bilayer dot.

In order to determine the structure of this newly obtained γ' - Fe_4N , a typical height profile of the surface was recorded as shown in Fig. 4(d). It is clear that the new structure is higher than both the Cu surface and the surface including the monolayer/dot-like bilayer γ' - Fe_4N . This suggests that the new area is composed of γ' - Fe_4N thicker than bilayer. Quantitative information on the thickness of the new structure could be obtained from Fe $L(2p \rightarrow 3d)$ edge jump spectra shown in Fig. 4(e), whose intensity is roughly proportional to the amount of surface/subsurface Fe atoms. The sample prepared in the same procedure as that shown in Fig. 4(b) reveals an edge jump value of 0.32, while the monolayer γ' - Fe_4N 0.12³⁹. Considering that the new area occupies $\sim 60 \%$ of the entire surface as deduced from Fig. 4(b), the thickness of this γ' - Fe_4N must be less than quadlayer to meet the experimental edge jump value of 0.32 (See Appendix A). Hence, the newly obtained structure is identified as a trilayer γ' - Fe_4N film. An atomic structure expected for the trilayer γ' - Fe_4N on $\text{Cu}(001)$ is presented in Fig. 4(f). The growth without any ion bombardment to the monolayer surface possibly stabilizes the subsurface pure Fe layer, which could promote the formation of the trilayer γ' - Fe_4N film in a

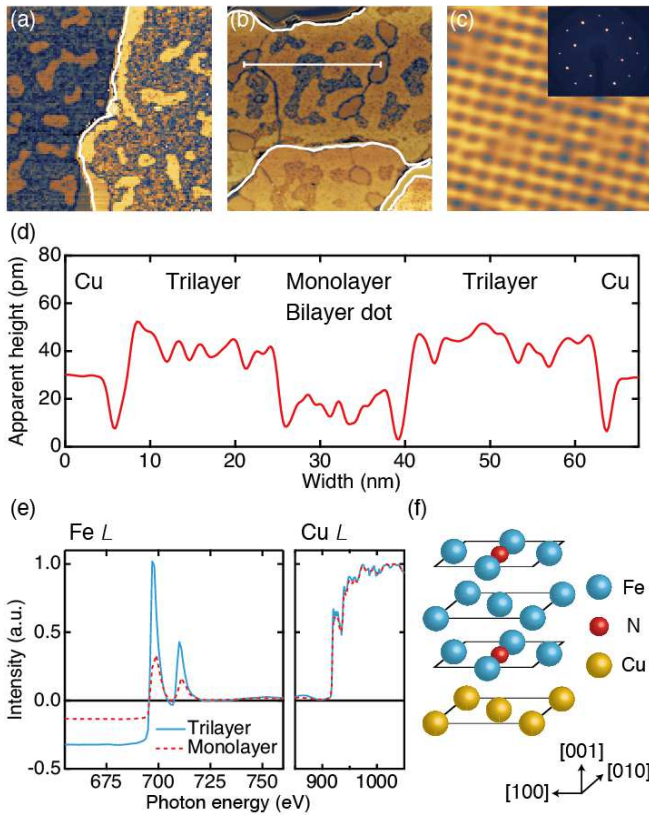


FIG. 4. (Color online) Topography of the trilayer γ' -Fe₄N film on Cu(001). Topographic images (100×100 nm²) after (a) two and (b) three cycles of the Fe deposition under N₂ atmosphere and subsequent annealing onto the monolayer γ' -Fe₄N on Cu(001). The setpoint is $I = 0.1$ nA, $V_s = -0.1$ V for (a) and -0.05 V for (b). White lines indicate step edges of the Cu terraces. Color contrast is enhanced within each terrace. (c) Atomically-resolved topographic image (4×4 nm², $I = 5.0$ nA, $V_s = -0.1$ V) of the trilayer γ' -Fe₄N surface. An inset represents a LEED pattern of the sample shown in (b), obtained with an incident electron energy of 100 eV. (d) Height profile measured along the line indicated in (b). (e) XAS edge jump spectra of the trilayer (solid) and monolayer (dotted) samples at the Fe and Cu *L* edges. The intensity is normalized to the Cu edge jump. (f) Atomic model expected for the trilayer γ' -Fe₄N on Cu(001). Blue (yellow) large and red small spheres represent Fe (Cu) and N atoms, respectively.

large area.

Finally, let us mention another growth method of the γ' -Fe₄N film. We previously report a possible layer-by-layer growth of the γ' -Fe₄N atomic layers on Cu(001), by the N⁺ ion bombardment with a relatively low energy of 0.15 keV⁴⁰. This soft implantation of N⁺ ions successfully avoids extra damage to the existing γ' -Fe₄N structures during the repetition of the growth cycles. The reported different electronic/magnetic states could then originate from the difference in the fabrication processes. Another finding is that, in the current study, only the monolayer and trilayer γ' -Fe₄N could be obtained in a continuous film form. This implies that an

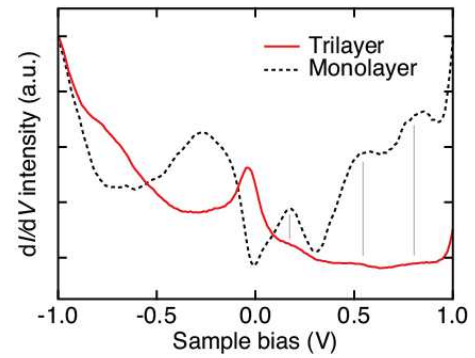


FIG. 5. (Color online) Surface electronic structures of the γ' -Fe₄N on Cu(001). Experimental dI/dV spectra recorded above the trilayer (solid) and monolayer (dotted) γ' -Fe₄N surfaces are presented. The dI/dV intensity is arbitrary. A STM tip was stabilized at $V_s = +1.0$ V, $I = 3.0$ and 7.0 nA for the trilayer and monolayer surfaces, respectively. Gray lines are guide to the eye.

Fe₂N-layer termination would be preferable through the present methods, possibly due to the metastability of an interface between Cu and pure Fe layers³⁴⁻³⁷.

C. Electronic and magnetic properties of γ' -Fe₄N atomic layers

The surface electronic structures of γ' -Fe₄N showed large dependence on the sample thickness. Figure 5 displays experimental dI/dV spectra measured on the surfaces of the trilayer and monolayer γ' -Fe₄N. The peaks located at $V_s \sim +0.20$, $+0.55$, and $+0.80$ V, mainly originating from the unoccupied states in the down-spin band characteristic of Fe local density of states (LDOS), are observed for both the trilayer and monolayer surfaces. A significant difference between the spectra is a dominant peak located around $V_s = -50$ mV observed only for the trilayer surface. This peak possibly originates from the LDOS peak located around $E - E_F = -0.2$ eV, calculated for the Fe atoms not bonded to N atoms in the subsurface Fe layer [corresponding site of Fe4 shown in Fig. 7(b)]. Because of the $d_{3z^2-r^2}$ orbital character, this peak could be dominantly detected in the STS spectrum for the trilayer surface. Thus, the appearance of this additional peak could support the different subsurface structure of the trilayer sample, especially, the existence of the subsurface Fe layer proposed above.

The entire electronic and magnetic properties of the sample, including both surface and subsurface information, were investigated by using XAS and XMCD techniques at the Fe *L*_{2,3} ($2p_{1/2,3/2} \rightarrow 3d$) absorption edges. Figure 6(a) shows XAS (μ_+ , μ_-) and XMCD ($\mu_+ - \mu_-$) spectra under $B = \pm 5$ T of the trilayer and monolayer samples in the grazing ($\theta = 55^\circ$) and normal

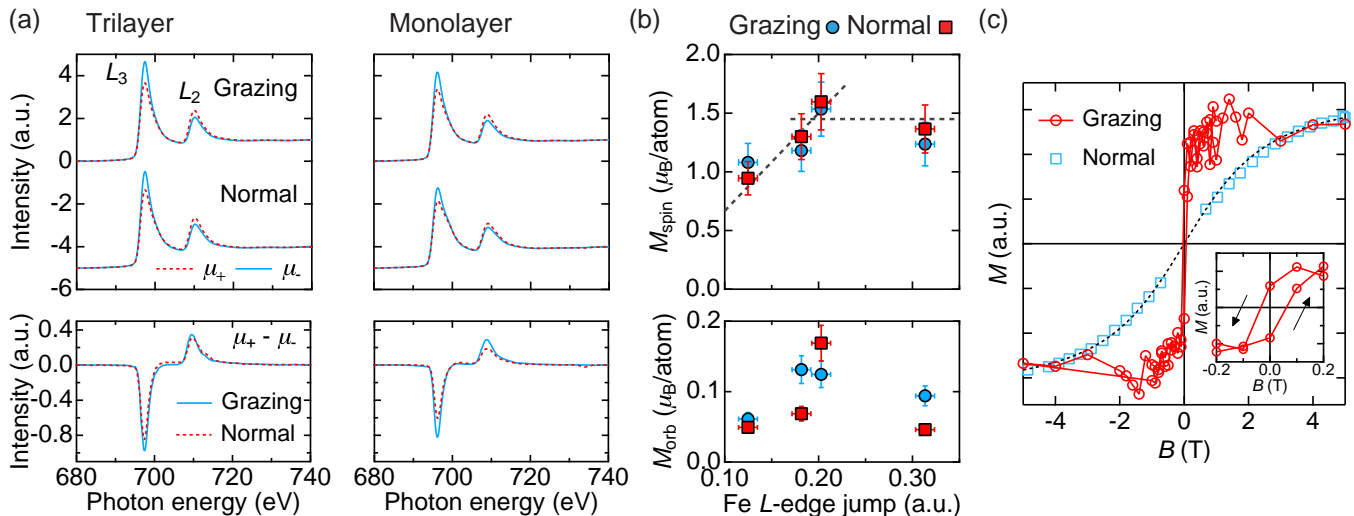


FIG. 6. (Color online) Thickness-dependent electronic and magnetic properties of the γ' -Fe₄N atomic layers on Cu(001). (a) Upper panels: XAS spectra under $B = \pm 5$ T of the trilayer (left) and monolayer (right) samples in the grazing (top) and normal (bottom) incidence. Lower panels: Corresponding XMCD spectra in the grazing (solid) and normal (dotted) incidence. All the spectra are normalized to the Fe XAS L -edge jump. (b) Upper [lower] panel: Experimental spin [orbital] magnetic moment in the grazing (circle) and normal (square) incidence plotted with respect to the Fe L -edge jump values. The edge jump values of 0.12 and 0.32 correspond to those of the monolayer and trilayer samples, respectively. Dotted lines are guide to the eye. Error bars are indicated to all the data, and smaller than the marker size if not seen. (c) Magnetization of the monolayer sample recorded in the grazing (circle and line) and normal (square) incidence. A dotted line is the guide to the eye. An inset shows an enlarged view of the curve recorded in the grazing incidence.

incidence ($\theta = 0^\circ$). Here, μ_+ (μ_-) denotes a x-ray absorption spectrum with the photon helicity parallel (antiparallel) to the Fe $3d$ majority spin, and an incident angle θ is defined as that between the sample normal and incident x-ray. The trilayer (monolayer) sample was prepared in the same procedure as that shown in Fig. 4(b) [Fig. 1(a)]. It is clear that the XMCD intensity is larger in the trilayer one, indicating an enhancement of magnetic moments with increasing thickness.

For a further quantitative analysis on the magnetic moments, we applied XMCD sum rules^{41,42} to the obtained spectra and estimated spin (M_{spin}) and orbital (M_{orb}) magnetic moments separately. Note that the average number of $3d$ holes (n_{hole}) of 3.2 was used in the sum-rule analysis, which was estimated by comparing the area of the experimental XAS spectra with that of a reference spectrum of bcc Fe/Cu(001) ($n_{\text{hole}} = 3.4$)⁴³. The thickness dependence of the M_{spin} and M_{orb} values is summarized in Fig. 6(b). The value of M_{spin} increases monotonously with increasing the Fe L -edge jump value, namely, an average sample thickness, and finally saturates at $\sim 1.4 \mu_B/\text{atom}$ in the trilayer sample (corresponding edge jump value of 0.32). The change in M_{orb} is not so systematic relative to M_{spin} , however, the M_{orb} values seem to be enhanced in the grazing incidence. This implies an in-plane easy magnetization of the γ' -Fe₄N atomic layers on Cu(001), also consistent with the previous reports on the γ' -Fe₄N thin films on Cu(001)^{8,40}. Figure 6(c) shows magnetization curves of the monolayer sample, whose intensity corresponds

TABLE I. Calculated atomic magnetic moments of the Fe atoms at each site (in units of μ_B/atom). The site notation is the same as that used in Fig. 7.

	Surface Fe ₂ N		Subsurface Fe		Interfacial Fe ₂ N	
	Fe1	Fe2	Fe3	Fe4	Fe5	Fe6
Monolayer	1.1	1.1	-	-	-	-
Trilayer	1.8	1.8	2.0	3.0	0.62	0.62

to the L_3 -peak XAS intensity normalized to the L_2 one. The curve recorded in the normal incidence shows negligible remanent magnetization. On the other hand, that in the grazing one draws a rectangular hysteresis loop, which confirms the in-plane easy magnetization. The coercivity of the monolayer sample is estimated to be ~ 0.05 T at 8.0 K, larger than ~ 0.01 T for 5 ML Fe/Cu(001)²¹, ~ 1 mT for 5 ML Fe/GaAs(100)-(4 \times 6)⁴⁴ and the 30 nm thick γ' -Fe₄N film⁸ at RT.

D. Theoretical analysis on the electronic and magnetic states of γ' -Fe₄N atomic layers on Cu(001)

The observed thickness dependence of the magnetic moments can be well understood with a help of first-principles calculations. Figures 7(a) and 7(b) show layer-resolved DOS of the monolayer and trilayer γ' -Fe₄N on Cu(001), respectively. Here, non-equivalent Fe sites in each layer are distinguished by different numbering.

In particular, the Fe atoms at the Fe3 (Fe4) site in the trilayer γ' -Fe₄N correspond to those with (without) a bond to N atoms⁴⁵. In Table I, calculated values of an atomic magnetic moment M_{atom} , corresponding to $M_{\text{spin}} + M_{\text{orb}}$ along the easy magnetization direction, are also listed. In the monolayer case, the calculated M_{atom} is 1.1 μ_{B} /atom, which is in perfect agreement with the experimental value. This supports an ideal atomic structure of our monolayer sample.

Interestingly, the value of M_{atom} for the Fe atoms in the monolayer γ' -Fe₄N is more than 1.5 times smaller than that in the topmost layer of the trilayer one (1.83 μ_{B} /atom). In comparison with the DOS shown at the top of Fig. 7(b), the impact of the hybridization with the Cu states on the Fe DOS can be seen in Fig. 7(a): First, the DOS in the up-spin band, especially with $d_{3z^2-r^2}$ and d_{yz} orbitals, becomes to have a tail toward a higher-energy side across the E_{F} . This change deviates the 3d electrons in the up-spin band from a fully-occupied nature. Moreover, the spin asymmetry of the occupied 3d electrons, the difference between the electron occupation into each spin band normalized by the sum of them, reduces especially for the DOS with d_{xy} , $d_{3z^2-r^2}$ and d_{yz} orbitals. These changes could decrease M_{spin} of the Fe atoms. Note that the similar reduction in the magnetic moments of 3d TMs due to the hybridization with Cu states is reported, for example, in Ref. 46 and 47.

Then, by comparing two different Fe₂N interfaces with the Cu substrate, it turns out that M_{atom} of the monolayer γ' -Fe₄N (1.1 μ_{B} /atom) is almost twice compared to that of the trilayer one (0.62 μ_{B} /atom). In the monolayer case, the Fe₂N layer faces to a vacuum and the Fe atoms are under reduced atomic coordination. This results in the narrower band width, and thus the DOS intensity increases in the vicinity of E_{F} . Accordingly, a larger exchange splitting can be possible and the spin asymmetry of the occupied 3d electrons increases as shown in Fig. 7(a), compared to the interfacial Fe₂N layer of the trilayer γ' -Fe₄N [bottom panel of Fig. 7(b)]. This leads to larger magnetic moments at the surface. As a result, the competition between the enhancement at the surface and the decrease at the interface would make M_{atom} values quite layer-sensitive.

In the subsurface Fe layer of the trilayer γ' -Fe₄N, the value of M_{atom} becomes largest due to the bulk coordination of the Fe atoms. Especially the Fe atoms not bonded to the N ones possess M_{atom} of 3.0 μ_{B} /atom, which is comparable to the values of Fe atoms at the same site in the bulk γ' -Fe₄N². Consequently, by averaging the layer-by-layer M_{atom} values of the trilayer γ' -Fe₄N, the total magnetic moment detected in the XMCD measurement is expected to be 1.7 μ_{B} /Fe, with the electron escape depth taken into account (See Appendix A). Considering the composition expected to the trilayer sample, this value can well explain the experimental one of ~ 1.5 μ_{B} /Fe.

The theory also demonstrates the direction of an easy

magnetization axis. The in-plane easy magnetization of our γ' -Fe₄N samples was confirmed by the magnetization curves as well as the incidence dependence of the M_{orb} value. In contrast, the pristine ultrathin Fe films, which form either fct or fcc structures on Cu(001), show uncompensated out-of-plane spins over a few surface layers^{24,48}. This shift of magnetic anisotropy by nitridation can be understood from the orbital-resolved Fe DOS shown in Figs. 7(a) and 7(b). Unlike the pure Fe/Cu(001) system⁴⁹, the occupation of 3d electrons in states with out-of-plane-oriented orbitals (d_{yz} , d_{zx} , $d_{3z^2-r^2}$) is considerably larger than that with in-plane-oriented ones (d_{xy} , $d_{x^2-y^2}$). This could make M_{orb} prefer to align within a film plane, resulting in the in-plane magnetization of the system⁵⁰.

IV. SUMMARY

In conclusion, we have conducted a detailed study on the growth, electronic and magnetic properties of the γ' -Fe₄N atomic layers on Cu(001). The ordered trilayer film of γ' -Fe₄N can be prepared by the Fe deposition under N₂ atmosphere onto the existing monolayer surface. On the other hand, the repetition of the growth cycles including the high-energy N⁺ ion implantation resulted in the imperfect bilayer γ' -Fe₄N. The STM and STS observations revealed the change in the surface topography and electronic structures with increasing the sample thickness. The XAS and XMCD measurements also showed the thickness dependence of the spectra, and the corresponding evolution of the M_{spin} values. All the thickness dependence of the electronic and magnetic properties is well explained by the layer-resolved DOS calculated using the first principles. Structural perfection of the system makes it possible to fully comprehend the layer-by-layer electronic/magnetic states of the γ' -Fe₄N atomic layers.

V. ACKNOWLEDGEMENT

This work was partly supported by the JSPS Grant-in-Aid for Young Scientists (A), Grant No. 16H05963, for Scientific Research (B), Grant No. 26287061, the Hoso Bunka Foundation, Shimadzu Science Foundation, Iketani Science and Technology Foundation, and Nanotechnology Platform Program (Molecule and Material Synthesis) of the Ministry of Education, Culture, Sports, Science and Technology (MEXT), Japan. Y. Takahashi was supported by the Grant-in-Aid for JSPS Fellows and the Program for Leading Graduate Schools (MERIT). A.E. acknowledges funding by the German Research Foundation (DFG Grants No. ER 340/4-1).

Appendix A: Conversion of XAS edge jump values to the thickness of γ' -Fe₄N

The escape probability of electrons from inside a sample to a vacuum depends on the depth at which the electrons are excited. For a numerical interpretation of the XAS edge jump, the following factors should be mainly considered in principle: the penetration length of an incident x-ray (λ_x) and electron escape depth (λ_e), both energy-dependent. In the case of a few atomic layers of 3d transition metals, the attenuation of the incident x-ray intensity is almost negligible because λ_x is orders of magnitude longer than the sample thickness⁵¹. Therefore, in the present case, only the electron escape probability at the depth z from the surface, namely, a factor of $\exp(-z/\lambda_e)$ is taken into account. As for the λ_e value of Fe, 17 Å was tentatively assumed in our analysis, which

is experimentally determined for Fe thin films⁵¹. Then, based on the experimental Fe (N) edge jump values of 0.12 (0.015), those for the full-coverage dot-like bilayer, trilayer, and quadlayer γ' -Fe₄N on Cu(001) are calculated as summarized in Table II.

TABLE II. Experimental and calculated Fe (N) edge jump values for the monolayer, dot-like bilayer, trilayer, and quadlayer γ' -Fe₄N on Cu(001). In the calculation, each γ' -Fe₄N is assumed to have the atomic structure presented in the text and fully cover the entire surface. For the quadlayer one, an Fe₂N/Fe₂/Fe₂N/Fe₂/Cu(001) structure is assumed.

	Fe edge jump		N edge jump	
	Experiment	Calculation	Experiment	Calculation
Monolayer	0.12 (exp.)		0.015 (exp.)	
Bilayer dot	-	0.19	-	0.015
Trilayer	0.32	0.40	0.032	0.034
Quadlayer	-	0.57	-	0.034

- * toshio.miyamachi@issp.u-tokyo.ac.jp
† komori@issp.u-tokyo.ac.jp
- ¹ J. Coey and P. Smith, *J. Magn. Magn. Mater.* **200**, 405 (1999).
 - ² B. C. Frazer, *Phys. Rev.* **112**, 751 (1958).
 - ³ J. M. D. Coey, *J. Appl. Phys.* **76**, 6632 (1994).
 - ⁴ M. Komuro, Y. Kozono, M. Hanazono, and Y. Sugita, *J. Appl. Phys.* **67**, 5126 (1990).
 - ⁵ C. Ortiz, G. Dumpich, and A. H. Morrish, *Appl. Phys. Lett.* **65**, 2737 (1994).
 - ⁶ S. Atiq, H.-S. Ko, S. A. Siddiqi, and S.-C. Shin, *Appl. Phys. Lett.* **92**, 222507 (2008).
 - ⁷ D. M. Borsa, S. Grachev, D. O. Boerma, and J. W. J. Kerssemakers, *Appl. Phys. Lett.* **79**, 994 (2001).
 - ⁸ J. M. Gallego, S. Y. Grachev, D. M. Borsa, D. O. Boerma, D. Écija, and R. Miranda, *Phys. Rev. B* **70**, 115417 (2004).
 - ⁹ K. Ito, G. H. Lee, K. Harada, M. Suzuno, T. Suemasu, Y. Takeda, Y. Saitoh, M. Ye, A. Kimura, and H. Akinaga, *Appl. Phys. Lett.* **98**, 102507 (2011).
 - ¹⁰ K. R. Nikolaev, I. N. Krivorotov, E. D. Dahlberg, V. A. Vas'ko, S. Urazhdin, R. Loloe, and W. P. Pratt, *Appl. Phys. Lett.* **82**, 4534 (2003).
 - ¹¹ S. Kokado, N. Fujima, K. Harigaya, H. Shimizu, and A. Sakuma, *Phys. Rev. B* **73**, 172410 (2006).
 - ¹² K. Ito, K. Toko, Y. Takeda, Y. Saitoh, T. Oguchi, T. Suemasu, and A. Kimura, *J. Appl. Phys.* **117**, 193906 (2015).
 - ¹³ C.-M. Fang, R. S. Koster, W.-F. Li, and M. A. van Huis, *RSC Adv.* **4**, 7885 (2014).
 - ¹⁴ S. H. Kim, K. S. Lee, H. G. Min, J. Seo, S. C. Hong, T. H. Rho, and J.-S. Kim, *Phys. Rev. B* **55**, 7904 (1997).
 - ¹⁵ F. Nouvertné, U. May, M. Bammig, A. Rampe, U. Korte, G. Güntherodt, R. Pentcheva, and M. Scheffler, *Phys. Rev. B* **60**, 14382 (1999).
 - ¹⁶ P. Torelli, F. Sirotti, and P. Ballone, *Phys. Rev. B* **68**, 205413 (2003).
 - ¹⁷ P. Srivastava, N. Haack, H. Wende, R. Chauvistré, and K. Baberschke, *Phys. Rev. B* **56**, R4398 (1997).
 - ¹⁸ M. Farle, W. Platow, A. N. Anisimov, P. Pouloupoulos, and K. Baberschke, *Phys. Rev. B* **56**, 5100 (1997).
 - ¹⁹ M. Farle, B. Mirwald-Schulz, A. N. Anisimov, W. Platow, and K. Baberschke, *Phys. Rev. B* **55**, 3708 (1997).
 - ²⁰ B. Schulz and K. Baberschke, *Phys. Rev. B* **50**, 13467 (1994).
 - ²¹ D. Li, M. Freitag, J. Pearson, Z. Q. Qiu, and S. D. Bader, *Phys. Rev. Lett.* **72**, 3112 (1994).
 - ²² M. Straub, R. Vollmer, and J. Kirschner, *Phys. Rev. Lett.* **77**, 743 (1996).
 - ²³ W. Weber, A. Bischof, R. Allenspach, C. H. Back, J. Fassbender, U. May, B. Schirmer, R. M. Jungblut, G. Güntherodt, and B. Hillebrands, *Phys. Rev. B* **54**, 4075 (1996).
 - ²⁴ H. L. Meyerheim, J.-M. Tonnerre, L. Sandratskii, H. C. N. Tolentino, M. Przybylski, Y. Gabi, F. Yildiz, X. L. Fu, E. Bontempi, S. Grenier, and J. Kirschner, *Phys. Rev. Lett.* **103**, 267202 (2009).
 - ²⁵ T. Gejo, Y. Takata, T. Hatsui, M. Nagasono, H. Oji, N. Kosugi, and E. Shigemasa, *Chem. Phys.* **289**, 15 (2003).
 - ²⁶ T. Nakagawa, Y. Takagi, Y. Matsumoto, and T. Yokoyama, *Jpn. J. Appl. Phys.* **47**, 2132 (2008).
 - ²⁷ J. P. Perdew and Y. Wang, *Phys. Rev. B* **45**, 13244 (1992).
 - ²⁸ M. Lüders, A. Ernst, W. M. Temmerman, Z. Szotek, and P. J. Durham, *J. Phys.: Condens. Matter* **13**, 8587 (2001).
 - ²⁹ M. Geilhufe, S. Achilles, M. A. Köbis, M. Arnold, I. Mertig, W. Hergert, and A. Ernst, *J. Phys.: Condens. Matter* **27**, 435202 (2015).
 - ³⁰ J. M. Gallego, D. O. Boerma, R. Miranda, and F. Ynduráin, *Phys. Rev. Lett.* **95**, 136102 (2005).
 - ³¹ Y. Takahashi, T. Miyamachi, K. Ienaga, N. Kawamura, A. Ernst, and F. Komori, *Phys. Rev. Lett.* **116**, 056802 (2016).
 - ³² J. M. Gallego, S. Y. Grachev, M. C. G. Passeggi, F. Sacharowitz, D. Ecija, R. Miranda, and D. O. Boerma, *Phys. Rev. B* **69**, 121404 (2004).
 - ³³ C. Navio, J. Alvarez, M. J. Capitan, D. Ecija, J. M. Gallego, F. Yndurain, and R. Miranda, *Phys. Rev. B* **75**,

- 125422 (2007).
- ³⁴ T. Detzel and N. Memmel, *Phys. Rev. B* **49**, 5599 (1994).
- ³⁵ N. Memmel and T. Detzel, *Surf. Sci.* **307**, 490 (1994).
- ³⁶ J. Shen, J. Giergiel, A. Schmid, and J. Kirschner, *Surf. Sci.* **328**, 32 (1995).
- ³⁷ G. Bayreuther, F. den Broeder, D. Chambliss, K. Johnson, R. Wilson, and S. Chiang, *J. Magn. Magn. Mater.* **121**, 1 (1993).
- ³⁸ We checked the ionization of nitrogen molecules/atoms without bombardment using an ion gun. The ion flux monitored for the Fe evaporator increased in proportion to the rise in the N₂ pressure, far below the parameters at which Fe started to be evaporated. This indicates the ionization of the N₂ molecules and/or N atoms around the evaporator possibly by thermal electrons created inside it. Then, the N⁺ and N₂⁺ ions could reach to the surface together with the evaporated Fe atoms, or iron nitride was already formed before landing.
- ³⁹ The amount of the Fe atoms detected in the edge-jump spectra was smaller than that expected from the initially deposited ones. This implies that a certain amount of Fe atoms, not participating in forming any γ' -Fe₄N structures, was embedded into the Cu substrate during annealing, at least several nms (probing depth in the TEY mode) below the surface.
- ⁴⁰ Y. Takagi, K. Isami, I. Yamamoto, T. Nakagawa, and T. Yokoyama, *Phys. Rev. B* **81**, 035422 (2010).
- ⁴¹ P. Carra, B. T. Thole, M. Altarelli, and X. Wang, *Phys. Rev. Lett.* **70**, 694 (1993).
- ⁴² B. T. Thole, P. Carra, F. Sette, and G. van der Laan, *Phys. Rev. Lett.* **68**, 1943 (1992).
- ⁴³ C. T. Chen, Y. U. Idzerda, H.-J. Lin, N. V. Smith, G. Meigs, E. Chaban, G. H. Ho, E. Pellegrin, and F. Sette, *Phys. Rev. Lett.* **75**, 152 (1995).
- ⁴⁴ Y. B. Xu, E. T. M. Kernohan, D. J. Freeland, A. Ercole, M. Tselepi, and J. A. C. Bland, *Phys. Rev. B* **58**, 890 (1998).
- ⁴⁵ The difference of DOS between (Fe1, Fe2) in the monolayer γ' -Fe₄N, (Fe1, Fe2) and (Fe5, Fe6) in the trilayer one is just a switch of the orbital assignment between d_{yz} and d_{zx} . Therefore, the DOS of Fe2 in the monolayer γ' -Fe₄N, Fe2 and Fe6 in the trilayer one is not presented here.
- ⁴⁶ J. Tersoff and L. M. Falicov, *Phys. Rev. B* **26**, 6186 (1982).
- ⁴⁷ O. Hjortstam, J. Trygg, J. M. Wills, B. Johansson, and O. Eriksson, *Phys. Rev. B* **53**, 9204 (1996).
- ⁴⁸ D. Pescia, M. Stampanoni, G. L. Bona, A. Vaterlaus, R. F. Willis, and F. Meier, *Phys. Rev. Lett.* **58**, 2126 (1987).
- ⁴⁹ R. Lorenz and J. Hafner, *Phys. Rev. B* **54**, 15937 (1996).
- ⁵⁰ P. Bruno, *Phys. Rev. B* **39**, 865 (1989).
- ⁵¹ R. Nakajima, J. Stöhr, and Y. U. Idzerda, *Phys. Rev. B* **59**, 6421 (1999).

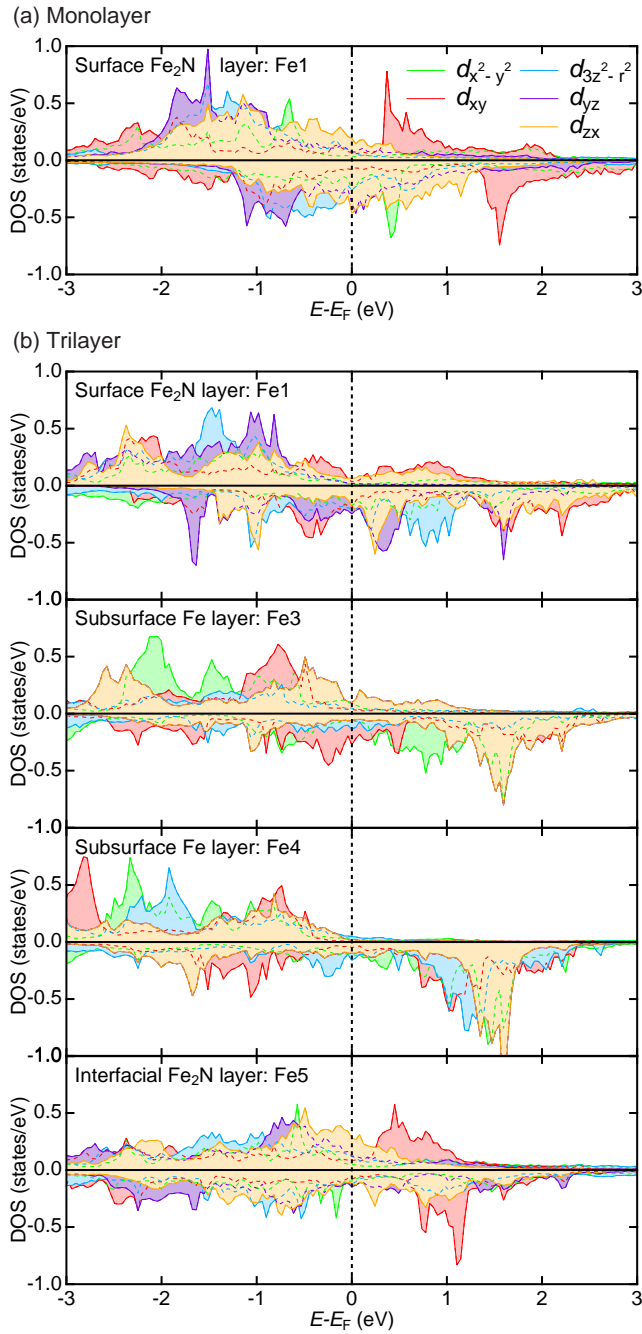


FIG. 7. (Color online) Layer-by-layer electronic states of the γ' -Fe₄N atomic layers on Cu(001). Calculated layer-resolved DOS projected to each 3d orbital of the (a) monolayer and (b) trilayer γ' -Fe₄N on Cu(001). The DOS in the up-(down-) spin band is shown at upper (lower) panels. Note that the states with d_{yz} and d_{zx} orbitals are degenerated for the Fe3 and Fe4 sites in (b).